From chaotic itinerancy to intermittent synchronization in complex networks

I. Leyva* and Irene Sendiña-Nadal
Complex Systems Group & GISC, Universidad Rey Juan Carlos, 28933 Móstoles, Spain
and Center for Biomedical Technology, Universidad Politécnica de Madrid, Pozuelo de Alarcón, 28223 Madrid, Spain

R. Sevilla-Escoboza
Centro Universitario de los Lagos, Universidad de Guadalajara, Lagos de Moreno, Jalisco, Mexico

V. P. Vera-Ávila
Instituto Politécnico Nacional, Unidad Profesional Interdisciplinaria de Ingeniería Campus Guanajuato, Guanajuato, Mexico

Christophe Letellier
Rouen Normandy University—CORIA, Avenue de l'Université, 76800 Saint-Etienne du Rouvray, France

(Received 19 November 2025; accepted 24 February 2026; published 26 March 2026)

Although synchronization has been extensively studied, key processes underlying its emergence in complex networks have remained hidden by the use of global order parameters. Here, we uncover how the route to synchronization unfolds through a sequential transition between two well-known but previously unconnected phenomena: *chaotic itinerancy* (CI) and *intermittent synchronization* (IS). Using a symbolic dynamics approach, we show that CI develops as a collective yet unsynchronized exploration of different domains of the high-dimensional attractor of the network, whose dimension is reduced as the coupling increases, ultimately collapsing into the reference chaotic attractor of an individual unit. At this stage, the IS emerges as irregular alternations between synchronous and asynchronous phases. These phenomena are mutually exclusive, each dominating a distinct coupling interval and governed by different mechanisms. Furthermore, network structural heterogeneity enhances itinerant behavior since access to different domains of the attractor depends on the nodes' topological roles. The CI-IS crossover occurs within a consistent coupling interval across models and topologies. Experiments on electronic oscillator networks confirm this two-step process, establishing a unified framework for understanding the route to synchronization in complex systems.

DOI: 10.1103/s3gp-gtln

I. INTRODUCTION

The study of collective dynamics in complex networks has advanced our understanding of how local interactions give rise to emergent behaviors such as synchronization, criticality, and pattern formation. Among these, synchronization has received the most attention, particularly in strongly coupled systems where coherent global states emerge. This emphasis, however, has often obscured the dynamical richness of weakly coupled systems, which remain largely unexplored despite their relevance to many natural and artificial systems. The brain is the most prominent example, where the role of synchronization and criticality in neural dynamics has long been recognized [1–4], and similar self-organized critical behavior has also been identified in other complex systems—from gene networks and ecosystems to artificial neural ensembles [5–7]. Operating near criticality allows such systems to balance robustness and sensitivity, maximizing adaptability and computational capacity [8].

When functioning away from global coherence, these systems display a rich repertoire of regimes and critical dynamics, including the two phenomena central to this work: *chaotic itinerancy* (CI) [9,10] and *intermittent synchronization* (IS) [11,12]. IS, observed at the edge of global synchronization, involves irregular alternations between coherent and unsynchronized phases [13,14]. This behavior corresponds to the well-known *on-off* intermittency [11,12] and has been reported in neural activity under both healthy and epileptogenic conditions [15,16]. IS thus provides a mechanism through which complex systems self-tune to operate near criticality, although its dependence on the underlying network structure remains poorly understood.

In contrast, CI refers to the trajectory within a high-dimensional attractor wandering through a sequence of metastable regimes (also known as *attractor ruins*) [17–19]. First introduced by Kaneko in nonequilibrium neural dynamics [20], CI has been observed across diverse contexts, including sensory processing in the olfactory cortex [10], perceptual switching in electroencephalographic (EEG) activity [21], laser dynamics [22,23], and adaptive robotic behavior [24–27]. In neural systems, metastable itinerant dynamics are

*Contact author: inmaculada.leyva@urjc.es

Published by the American Physical Society under the terms of the Creative Commons Attribution 4.0 International license. Further distribution of this work must maintain attribution to the author(s) and the published article's title, journal citation, and DOI.

thought to underlie cognitive processes such as working memory, decision making, and behavioral flexibility [8,28–32].

These features have also made CI relevant to machine learning and computation. Reservoir computing, for instance, exploits high-dimensional transients for memory and pattern classification, and recent work has demonstrated controlled CI in such architectures [33–36]. This supports the idea that transient, metastable dynamics are essential for flexible and context-dependent computation in both biological and artificial systems [8,19,32,37].

Although CI has been extensively investigated in globally coupled and random networks [9,20,34,36,38], its dependence on network topology remains largely unclear. Yet, real-world systems exhibiting CI typically feature modular, hierarchical, or heterogeneous architectures [19,39,40].

The main goal of this work is to address this gap. Specifically, we investigate how network topology influences the emergence, organization, and persistence of CI in weakly coupled oscillator systems, while clarifying its distinction from IS, as the two phenomena are often confounded [41]. We show that CI and IS occur as successive, mutually exclusive stages along the route to synchronization, each characterized by distinct critical behaviors. These properties prove robust across topologies, network sizes, and node dynamics, and are further validated through experiments on electronic oscillator networks.

To track CI, we propose a symbolic dynamics framework that encodes nodal trajectories into symbolic sequences, capturing transitions with higher sensitivity than standard time-averaged measures. This approach enables node-level analysis of visiting sequences and reveals how topological roles modulate access to different nodal regimes. By bridging a gap between network theory and nonlinear dynamics, it thus provides insights into how network topology shapes complex system behavior and may prove valuable for understanding computational and decision-making processes driven by chaotic itinerancy.

II. CHAOTIC ITINERANCY AND INTERMITTENT SYNCHRONIZATION

The route to synchronization in coupled oscillator networks is often characterized using global, time-averaged metrics such as the mean synchronization error or an order parameter that summarizes collective coherence. However, these global indicators often obscure the underlying, time-dependent phenomena occurring at the nodal level. In particular, they hide two critical yet interconnected processes: chaotic itinerancy and intermittent synchronization. CI corresponds to irregular transitions among metastable regimes at the node level, whereas IS manifests as intermittent alternations between synchronous and asynchronous phases at the network scale. Both phenomena emerge at weak-to-intermediate coupling strengths, revealing a multiscale organization that bridges nodal and network dynamics along the synchronization process.

To explore these regimes, we consider a network of N diffusively coupled identical chaotic oscillators governed by

$$\dot{\boldsymbol{x}}_i = \mathbf{f}(\boldsymbol{x}_i) - d\sum_{j=1}^{N} L_{ij}\,\mathbf{h}(\boldsymbol{x}_j), \tag{1}$$

where $\boldsymbol{x}_i \in \mathbb{R}^m$ is the state vector of the ith node; $\mathbf{f}$ and $\mathbf{h}$ are functions $\mathbb{R}^m \to \mathbb{R}^m$ describing the intrinsic dynamics of an isolated unit and the coupling interaction, respectively; d is the coupling strength; and L_{ij} is the Laplacian matrix encoding the network topology, with $L_{ij} = -1$ if nodes i and j are connected ($L_{ij} = 0$ otherwise), and $L_{ii} = k_i$ is the degree of the ith node.

This formulation captures a broad class of diffusive interactions and enables systematic tracking of multiscale organization underlying the synchronization process. The network behaves as a single dynamical system whose state space is $\mathbb{R}^{Nm}$, producing an attractor $\mathcal{A}(d) \subset \mathbb{R}^{Nm}$ that depends on the coupling strength d, with all other parameters held constant. Each node i is associated with an m-dimensional substate space $\mathbb{R}^m_i$ containing an attractor $\mathcal{A}_i(d) \subset \mathbb{R}^m_i$. When uncoupled ($d = 0$), these subattractors $\mathcal{A}_i(0)$ coincide with $\mathcal{A}_\mathrm{r}$, hereafter referred to as the *reference attractor*.

Along the work, numerical simulations of Eq. (1) were carried out in several systems using a fourth-order Runge-Kutta scheme with fixed time step $\Delta t = 0.01$. For each value of the coupling parameter d, the systems were integrated over time intervals spanning several thousand multiples of the characteristic timescale of the uncoupled unit, after discarding an extensive transient regime. Unless otherwise stated, results correspond to averages over 30 independent realizations with randomly chosen initial conditions uniformly distributed within the attractor basin. Network topologies were chosen to represent heterogeneous and homogeneous degree distributions. Heterogeneous networks were generated using the Barabási-Albert (BA) algorithm [42], while homogeneous cases included Erdös-Rényi (ER) graphs [43] with prescribed average degree $\langle k \rangle$ and complete, all-to-all (AA) graphs.

Figure 1 illustrates the two distinct collective dynamical regimes analyzed in this work, in a network of $N = 100$ diffusively coupled Rössler oscillators. Panel (a) shows the expected gradual decrease of the mean synchronization error

$$\langle E \rangle = \lim_{T\to\infty} \frac{1}{T}\int_0^T E(t)\,dt, \tag{2}$$

where

$$E(t) = \frac{2}{N(N-1)}\sum_{i<j} \|\mathbf{x}_i(t) - \mathbf{x}_j(t)\|^2 \tag{3}$$

is the instantaneous synchronization error. The two points highlighted in panel (a) are representative of the coupling interval along this trajectory for each respective regime. At weak coupling ($d = 0.08$, red circle), the network exhibits CI, illustrated in panel (b), where the maxima of the x variable for two arbitrary nodes (vertically shifted for clarity) display irregular transitions among metastable attractor domains. Meanwhile, the instantaneous synchronization error $E(t)$ [panel (d)] remains persistently large, without signs of intermittence. In contrast, at stronger coupling [$d = 0.28$, blue square in panel (a)], CI collapses. As shown in panel (c), the maxima of the x variable for the same two nodes reveal that both trajectories remain confined to the same chaotic attractor, without further itinerant switching. However, panel (e) shows that $E(t)$ exhibits intervals of near-perfect synchrony interrupted by desynchronization bursts, hallmarks of IS.

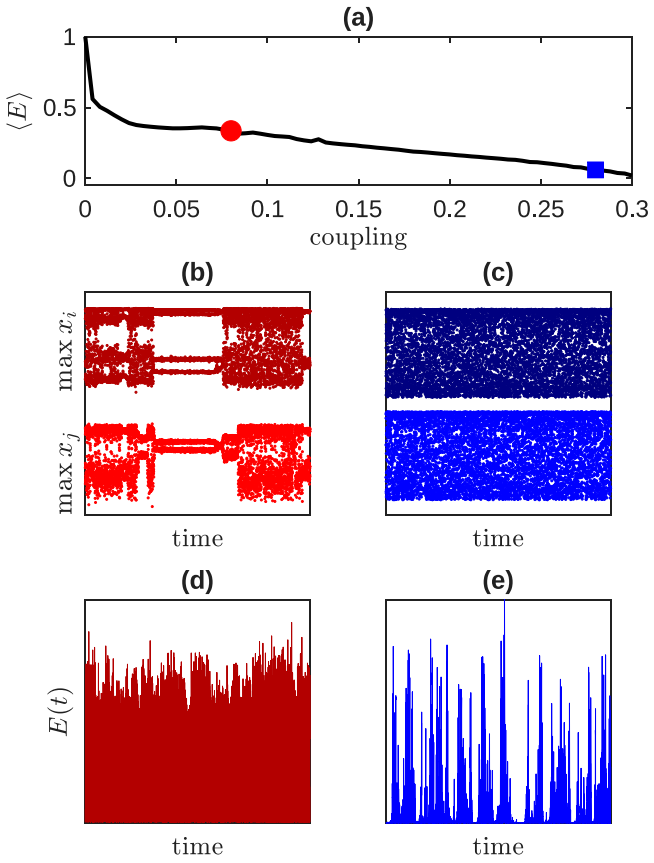


FIG. 1. Emergence of CI and IS along the route to synchronization in a network of $N = 100$ Rössler oscillators. (a) Mean synchronization error $\langle E \rangle$ as a function of the coupling strength d, highlighting two representative values: $d = 0.08$ (red circle, weak coupling) and $d = 0.28$ (blue square, strong coupling). (b), (c) Maxima of the x variable for two arbitrarily selected nodes (vertically shifted for clarity) at the coupling values indicated in panel (a). With a weak coupling [panel (b)], the dynamics exhibits CI, with irregular transitions among metastable regimes, whereas with a strong coupling [panel (c)], this itinerant wandering disappears and both nodes remain confined to the same chaotic regime. (d), (e) Instantaneous synchronization error $E(t)$ for the same coupling values. Only the strong-coupling case [panel (e)] displays IS with intervals where the synchronization error approaches zero, interrupted by desynchronization bursts. Model details: Rössler oscillators with $\mathbf{f}(\mathbf{x}) = [-y - z, x + ay, z(x - 4) + 2]$, $\mathbf{h}(\mathbf{x}) = [0, y, 0]$, and $a = 0.432$; heterogeneous network generated using the BA algorithm with average node degree $\langle k \rangle = 4$; initial conditions randomly chosen in the interval $\mathbf{x}_0 = [-0.5, 0.5]$.

Thus, along the same monotonic decrease of $\langle E \rangle$, the system transitions from a dynamics characterized by CI without IS to a dynamics where CI disappears, and IS emerges. Additional examples presented in the Supplemental Material (Fig. S1) illustrate the generality of these behaviors across different models and network structures [44].

These observations highlight the need for analytical tools that go beyond ensemble-averaged measures and capture the multiscale nature of these phenomena unfolding during the synchronization process. In the following subsections, we introduce two dedicated metrics: the CI and IS indexes.

A. Chaotic itinerancy index

Quantifying chaotic itinerancy in network dynamics is challenging due to the high-dimensional wandering trajectories involved [9,17,18]. Previous attempts have used Lyapunov exponents, recurrence plots, or entropy rates to detect transitions between metastable regimes [21,30,40,41,45]. However, these approaches largely rely on global or averaged measures, overlooking the heterogeneous and node-dependent nature of transitions in networked systems. To address this limitation, we introduce a symbolic dynamics framework that captures CI at the nodal level by tracking the sequence of transitions for each node individually. This approach reduces each node's time series to a discrete set of symbols representing regime sequences, enabling precise detection and quantification of transitions. The complete symbolic encoding procedure used throughout this work is summarized in the following pipeline, with each step illustrated in parallel in Fig. 2 for two nodes in a network of $N = 100$ Rössler oscillators:

(1) *Selection of scalar observable and sampling.* For each node i, a scalar time series $X_i = \{X_i(t_p)\}_{p=1}^{N_p}$ is extracted from its state vector $\mathbf{x}_i(t)$. For example, in Fig. 2 we use the sequence of the local maxima of the Rössler's x variable, obtained from crossings of the Poincaré section $\mathcal{P}_i = \{ x_i \in \mathbb{R} \mid \dot{x}_i = 0,\ x_i > 0 \}$, but alternative sampling schemes are equally compatible with the method (as uniform temporal sampling or other criteria).

(2) *Normalization.* Each series is rescaled to [0, 1] as $\hat{X}_i(t_p) = X_i(t_p)/\max(X_i)$, ensuring comparability across nodes and realizations.

(3) *Temporal partition.* The time series $\{X_i(t_p)\}$ are divided into N_τ consecutive windows of fixed number of D data points, such that $N_p = DN_\tau$. For visualization, panels (a)–(f) in Fig. 2 show the first 20 of these windows. Here, p indexes data points, while τ labels consecutive windows including D points, used for symbolic encoding.

(4) *Amplitude quantization.* The interval [0, 1] is uniformly partitioned into N_β amplitude bins [with $N_\beta = 6$ in Figs. 2(a) and 2(b)].

(5) *Visitation counts.* For each window $\tau \in \{1, \ldots, N_\tau\}$ and bin $\beta \in \{1, \ldots, N_\beta\}$, we compute $\pi_{\tau,\beta}^{(i)} \leqslant D$, the number of intersections falling in that bin.

(6) *Binary occupancy.* A (τ, β) cell is considered visited if the number of points $\pi_{\tau,\beta}^{(i)}$ falling within it exceeds a threshold $\theta_I \ll D$:

$$\Pi_{\tau,\beta}^{(i)} = \begin{cases} 1, & \text{if } \pi_{\tau,\beta}^{(i)} > \theta_I, \\ 0, & \text{otherwise}, \end{cases} \tag{4}$$

as shown in Figs. 2(c) and 2(d), where yellow indicates a visited cell and blue a nonvisited one.

(7) *Symbol definition.* The symbolic state of node i in window τ is

$$\sigma_\tau^{(i)} = \sum_{\beta=1}^{N_\beta} \Pi_{\tau,\beta}^{(i)}, \tag{5}$$

with $\sigma_\tau^{(i)} \in \{1, \ldots, N_\beta\}$, which captures the extent of attractor exploration during that window as shown in Figs. 2(e) and 2(f). Large values of $\sigma_\tau^{(i)}$ indicate trajectories spanning wide regions of the attractor, whereas small values correspond to

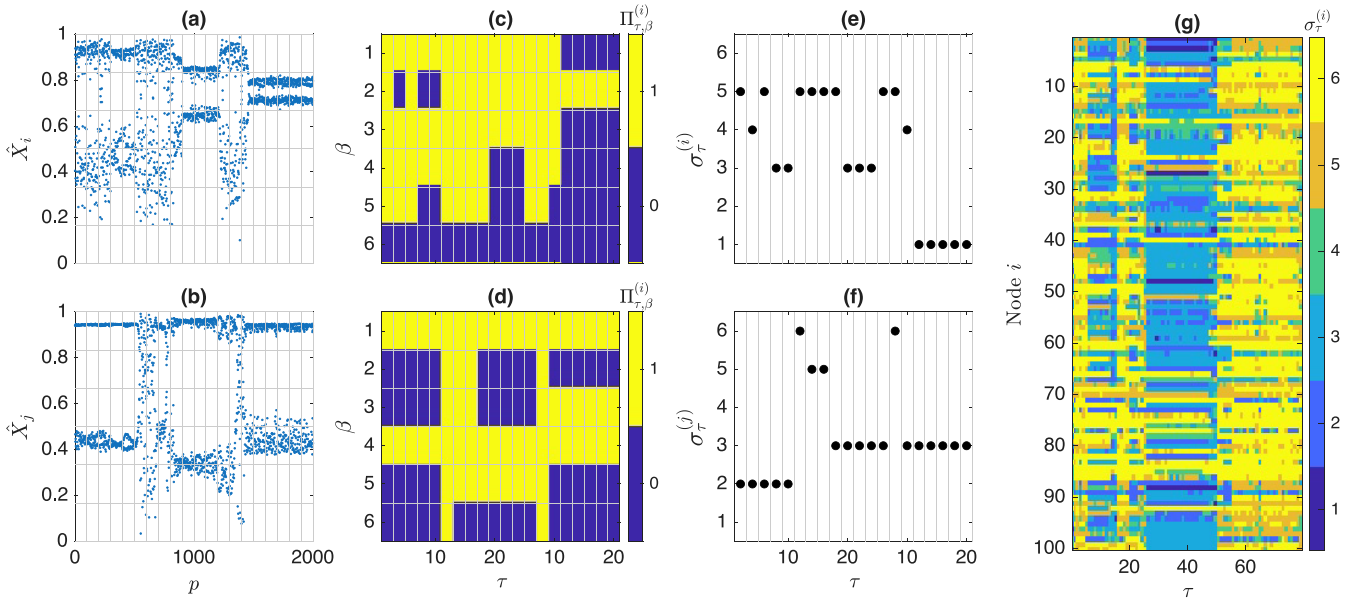


FIG. 2. Symbolic encoding procedure for characterizing chaotic itinerancy, illustrated for two arbitrary nodes in a network of coupled Rössler oscillators. (a), (b) Normalized sampled time series $\hat{X}_i$ and $\hat{X}_j$, corresponding to the scalar variables $X_i(t_p)$ and $X_j(t_p)$ of two arbitrary nodes where p indexes individual samples of the original time series. These sequences are obtained as maxima of the Rössler variable x. Data points are distributed over a grid (gray lines) of $N_\tau \times N_\beta$ cells, where each time window τ contains D consecutive samples. In this example, $D = 100$ and only 20 time windows (out of the total N_τ) are shown. (c), (d) Binary occupancy maps $\Pi^{(i)}_{\tau,\beta}$ for the nodes shown in panels (a) and (b). A cell (τ, β) is marked as visited ($\Pi^{(i)}_{\tau,\beta} = 1$, yellow) if it contains more than $\theta_I = 2$ points, and as empty ($\Pi^{(i)}_{\tau,\beta} = 0$, blue) otherwise. (e), (f) Symbolic state $\sigma^{(i)}_\tau$ for each time window, defined as the number of active cells visited by node i during window τ. Full exploration of the spatial partition corresponds to $\sigma^{(i)}_\tau = N_\beta = 6$. (g) Symbolic raster plot $\boldsymbol{\sigma} = \{\sigma^{(i)}_\tau\}$ showing the symbolic evolution of all N nodes in the network. The example corresponds to a heterogeneous degree distribution network of $N = 100$ coupled Rössler oscillators with coupling strength $d = 0.08$ and parameter $a = 0.432$.

confinement within near-periodic or low-developed chaotic regimes.

The robustness of the method with respect to the window parameters D and N_β is demonstrated in the Supplemental Material (Fig. S2), where the qualitative behavior of the symbolic dynamics remains stable over wide parameter ranges [44]. The window length D must be chosen in relation to the intrinsic timescales of the system: It should be larger than the number of intersections required for covering a duration greater than the Lyapunov time τ_L to ensure meaningful state-space exploration within each window, while remaining shorter than the typical residence time τ_{res} in a metastable regime in order to resolve genuine symbolic transitions. Similarly, the number of amplitude bins N_β is set to discretize the state-space exploration with sufficient granularity to distinguish dynamical regimes, while remaining insensitive to moderate parameter variations.

Applying the above procedure to all nodes yields a *symbolic raster plot* $\boldsymbol{\sigma} = \{\sigma^{(i)}_\tau\}$ [Fig. 2(g)], which encodes both the nodal diversity and the time variability in the network's dynamics.

The *chaotic itinerancy index* is then defined as the average number of transitions between symbolic states per node and per time window:

$$\Phi_\sigma = \frac{1}{N}\sum_{i=1}^{N}\left(\frac{1}{N_\tau - 1}\sum_{\tau=1}^{N_\tau - 1}\left[1 - \delta_{\sigma^{(i)}_{\tau+1},\sigma^{(i)}_\tau}\right]\right), \tag{6}$$

where δ_{ab} is the Kronecker delta. High values of Φ_σ indicate frequent transitions between metastable regimes—reflecting strongly itinerant trajectories—whereas low values correspond to dynamics confined to a single regime.

B. Intermittent synchronization index

Unlike chaotic itinerancy, the quantification of IS is a more established problem. On-off intermittence has been extensively studied in low-dimensional and small ensembles of coupled chaotic oscillators [13,46], whereas its manifestation in complex networks remains comparatively less explored [11,12]. Several approaches have been proposed to characterize this behavior, typically based on the statistics of laminar-phase durations, return maps, or burst amplitude distributions [14,47]. Here, rather than introducing an intermittency measure, we adopt a normalized definition that mirrors the structure of the CI index.

While Φ_σ quantifies CI by accounting for local transitions between metastable regimes, the corresponding *intermittent synchronization index* Φ_E is designed to reflect global alternations between coherent and incoherent network phases that define IS.

This index is computed from the instantaneous synchronization error $E(t)$ introduced in Eq. (3). The sampled signal $E(t_n)$ is binarized using a threshold θ_E and defined as $\varepsilon(t_n) = H(E(t_n) - \theta_E)$, where $H(x)$ denotes the Heaviside function

[11,12]. Here, $\varepsilon(t_n) = 0$ corresponds to synchronous phases, while $\varepsilon(t_n) = 1$ indicates desynchronized bursts. The threshold θ_E is typically chosen to be small (e.g., $\theta_E \sim 10^{-5}$), but may be adjusted according to the noise level.

The index is then defined as the normalized number of alternations between these two states:

$$\Phi_E = \frac{1}{N_t - 1} \sum_{n=1}^{N_t - 1} |\varepsilon(t_{n+1}) - \varepsilon(t_n)|, \tag{7}$$

where N_t is the total number of data points.

Large values of Φ_E indicate frequent switching between coherent and noncoherent phases—hallmarks of on-off intermittency—whereas $\Phi_E = 0$ corresponds to either complete incoherence or full synchronization. Thus, Φ_E measures the instability of the laminar phases rather than the absolute level of coherence.

Together, the two indices, Φ_σ and Φ_E, provide complementary quantitative descriptions of nodal-level (CI) and network-level (IS) dynamics that organize the route to synchronization in complex networks.

III. SEQUENTIAL ONSET OF CI AND IS

To investigate the onset and development of CI and its relation to IS, we first examine the route to synchronization in an ensemble of $N = 100$ identical Rossler oscillators arranged on a heterogeneous undirected network with average degree $\langle k \rangle = 4$. This topology provides sufficient degree heterogeneity and is large enough to prevent the emergence of global periodic regimes, allowing us to focus on the genuinely chaotic itinerant dynamics that arise during synchronization. Statistical robustness is ensured by sampling a large set of initial conditions for the oscillator states.

Figure 3(a) reports the evolution of the CI index Φ_σ (red) and the IS index Φ_E (blue) as functions of the coupling strength d, alongside the synchronization error E (green) as a reference for global coherence. A key observation is that Φ_σ and Φ_E activate sequentially and do not coexist: Itinerancy emerges immediately at low couplings and grows rapidly, reflecting the onset of a collective exploration of metastable regimes. The CI index reaches a peak and then gradually declines as oscillators converge toward the same symbolic state, corresponding to the reference chaotic attractor $\mathcal{A}_\mathrm{r}$.

Only after this contraction does IS appear, signaling the final stage of the synchronization process (around $d \sim 0.2$ in the example). During the IS regime, near-synchronous periods are interrupted by global desynchronization bursts, consistent with previous findings [11,12]. Here, IS is reinterpreted as the natural continuation of CI collapse: all nodes settled on the reference attractor $\mathcal{A}_\mathrm{r}$, but not in a synchronous way. The sequential emergence of these two regimes—first CI, then IS—is a central contribution of this work.

A complementary view of the sequential onset of CI and IS comes from the Lyapunov spectrum of the full $3N$-dimensional system. We computed the spectrum using the standard Benettin algorithm [48] with Gram-Schmidt reorthonormalization on the tangent space of the network dynamics, following the procedure in Ref. [49]. The N largest

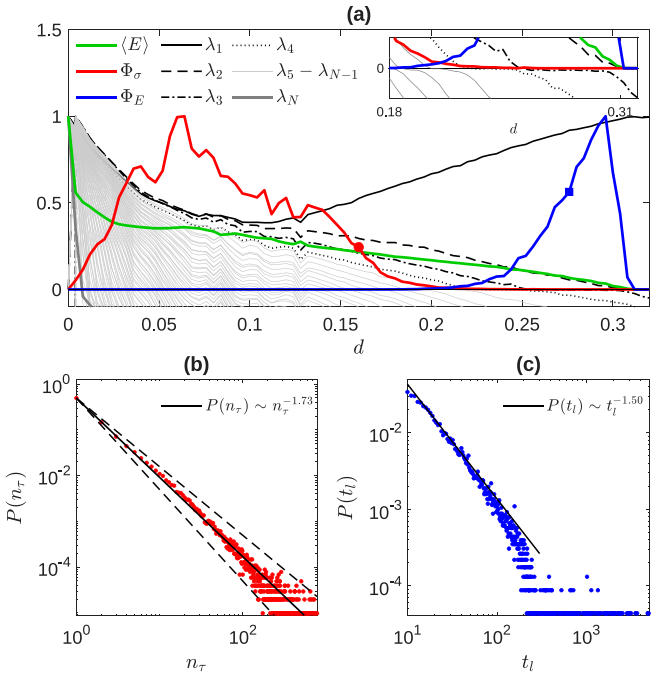


FIG. 3. Synchronization route and emergence of CI and IS in a heterogeneous network (generated with the BA algorithm, $\langle k \rangle = 4$) of $N = 100$ chaotic Rössler oscillators. (a) Global synchronization error $\langle E \rangle$ (green), chaotic itinerancy index Φ_σ (red), and intermittent synchronization index Φ_E (blue) as functions of the coupling strength d. The N largest Lyapunov exponents are also shown in various shades of gray and line styles as indicated in the legend. The inset highlights the coupling interval where CI vanishes and gives rise to IS until the system reaches global synchrony with $\lambda_1 > 0$, $\lambda_2 = 0$, and $\lambda_3 < 0$. (b) Log-log probability distribution of the residence duration n_τ in the most developed chaotic symbolic state $\sigma = N_\beta$, at $d = 0.16$ [red circle in panel (a)], exhibiting power-law behavior. The solid straight line shows the best fit to a power law $P(n_\tau) \sim n_\tau^{-1.73}$, while dashed lines indicate bounds with exponents 2 (upper) and 1.5 (lower). (c) Log-log probability distribution of the coherent phase durations t_ℓ during IS, at $d = 0.27$ [blue square in panel (a)], following the scaling $P(t_\ell) \sim t_\ell^{-3/2}$ typical of on-off intermittency. Ensemble averages are computed over 30 independent sets of initial conditions. Rest of parameters: $D = 200$, $N_\beta = 6$, and $\theta = 3$.

Lyapunov exponents are shown in Fig. 3(a) (shaded gray), overlaid on the CI and IS indicators. CI persists while the exponents λ_N through λ_4 become negative sequentially, indicating a progressive reduction in effective dimension that enables wandering across different metastable regimes. When λ_4 reaches zero [around $d \sim 0.22$ in this example; see inset in Fig. 3(a)], CI collapses, as signaled by the vanishing of Φ_σ. At this point, the synchronization process begins, and the IS index Φ_σ rises as the system fluctuates near the synchronous manifold, sustained by the remaining marginal direction $\lambda_3 \sim 0$. The final collapse occurs when simultaneously $\lambda_3 < 0$ and $\lambda_2 = 0$, leaving $\mathcal{A}(d)$ topologically equivalent to the reference attractor $\mathcal{A}_\mathrm{r}$.

Equivalently, the Lyapunov spectrum allows computing the Lyapunov dimension of the attractor as a function of coupling, $\mathcal{D}_\mathrm{L}(d)$, via the Kaplan-Yorke conjecture [50]. From this point

of view, CI occurs in the interval $\mathcal{D}_{\rm L}(0) = N\mathcal{D}_{\rm r} > \mathcal{D}_{\rm L}(d) > 4$, where $\mathcal{D}_{\rm r} = 2.03$ is the Lyapunov dimension of $\mathcal{A}_{\rm r}$ for the chosen parameters. Then, IS is observed in the subsequent range $4 \geqslant \mathcal{D}_{\rm L}(d) \geqslant \mathcal{D}_{\rm r}$. For this Rössler network, CI is only possible when the dynamics can be embedded in a space of dimension at least 5.

The correlation between near-zero Lyapunov exponents and the occurrence of CI or IS has been discussed in previous works [17,45,51–53], yet a clear distinction between these two regimes and their specific correspondence with the Lyapunov spectrum in large-scale systems has remained elusive.

To assess criticality in CI and IS, we analyze the distribution of residence durations within the symbolic state corresponding to the reference attractor $\mathcal{A}_{\rm r}$, encoded by the highest symbolic value $\sigma_i^\tau = N_\beta$. For each node, we measure the residence duration n_τ during which it remains in N_β before switching to another symbol. Figure 3(b) shows that the resulting distribution—averaged over all nodes and realizations—follows a power-law decay, $P(n_\tau) \sim n_\tau^{-1.7}$, for d approaching 0.22, the coupling value at which CI ceases. The emergence of this scaling precisely at the point where the itinerant dynamics collapses supports its interpretation as a critical transition: As nodes diminish their exploration of different regimes, their temporal organization becomes scale-free. Similar power-law residence-time distributions have been reported in deterministic [41] and stochastic [54] models of CI, where nodes' trajectories wander among regimes, though without explicitly identifying this final critical stage.

An analogous analysis was performed for IS. Here, the relevant residence time corresponds to the duration of synchronized phases, defined as intervals during which the global synchronization error $E(t)$ remains below a small threshold before a desynchronization burst occurs. Figure 3(c) shows that the distribution of these synchronized phases durations t_ℓ [measured at $d = 0.27$, blue circle in Fig. 3(a)] follows a power-law scaling, $P(t_\ell) \sim t_l^{-1.5}$, consistent with the universal exponent reported for on-off intermittency [13,14,55–57].

To further assess the consistency of the CI-IS sequence, we compared systems with different network architectures and node dynamics. Specifically, we analyzed networks with degree distributions ranging from complete graphs to power law, system sizes from $N = 5$ to 500 nodes, and distinct oscillator models, including the Lorenz system ($\mathbf{f}(\mathbf{x}) = [-10(y - x), x(28 - z) - y, xy - 2z]$, $\mathbf{h}(\mathbf{x}) = [0, y, 0]$, initial conditions in the range $\mathbf{x}_0 = [0, 10]$). In the latter case, the analyzed data were obtained via regular periodic sampling of x-variable time series, rather than Poincaré sections, using $D = 100$ and $N_\beta = 2$, adapted to the different timescales and state-space structure.

Figure 4 shows that when the coupling strength d is rescaled by the corresponding critical synchronization threshold d_c of each system, the crossover between itinerant and intermittent regimes, identified by the intersection of Φ_σ and Φ_E, consistently occurs at approximately $d/d_c \simeq 2/3$ across all cases. This robust scaling suggests a general organizational principle in the route to synchronization: Regardless of nodal dynamics or network topology, the system transitions from locally itinerant to globally intermittent dynamics at the same relative point along the path to coherence.

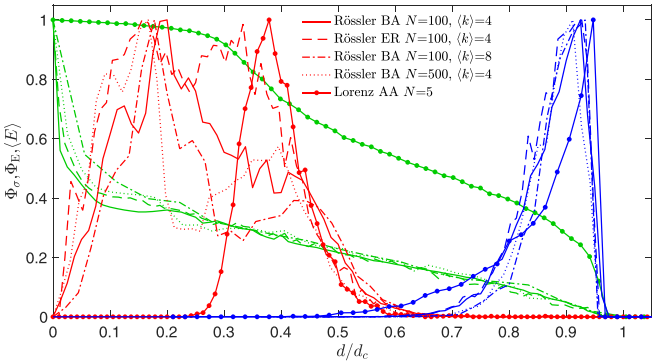


FIG. 4. Comparison of the chaotic itinerancy index Φ_σ (red) and the intermittent synchronization index Φ_E (blue) for networks with heterogeneous (BA) and homogeneous (ER and all-to-all) degree distributions, different average degrees ($\langle k\rangle = 4, 8$), system sizes ($N = 5, 100, 500$), and dynamical units (Rössler and Lorenz oscillators), distinguished by line styles as indicated in the legend. The corresponding mean synchronization error $\langle E\rangle$ (green) is also shown. In all cases, the coupling strength d is normalized by the critical synchronization threshold d_c of each network. Despite the diversity of topologies and node dynamics, the crossover between itinerant and intermittent regimes consistently occurs at $d/d_c \approx 2/3$.

IV. CI NODAL STRUCTURE

The symbolic dynamics introduced in Sec. II A not only provides a quantitative characterization of CI but also enables a detailed analysis of how the network's nodal structure shapes this phenomenon. By encoding each node's trajectory into N_β symbols, we can directly assess how structural heterogeneity influences the access and persistence of nodes within distinct regimes of the attractor $\mathcal{A}(d)$.

Figure 5(a) illustrates the evolution of symbolic occupation statistics across the coupling range where CI develops. The

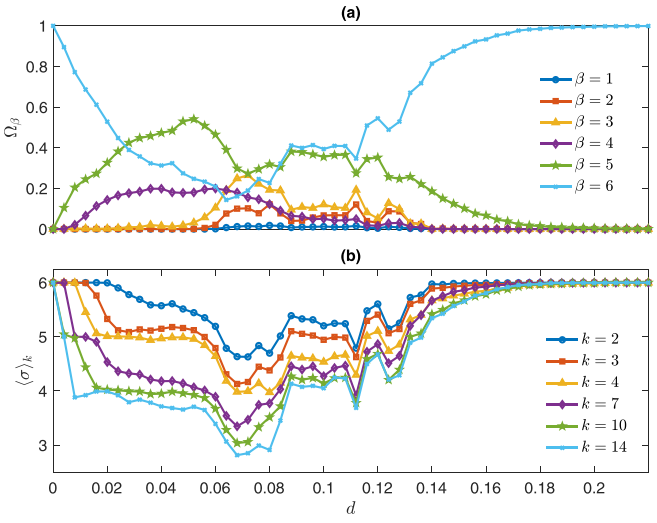


FIG. 5. Symbolic state analysis for the network used in Fig. 3. (a) Realization probability of each symbol Ω_β for $\beta = 1, \ldots, N_\beta = 6$, and (b) average symbolic state per degree class, $\langle\sigma\rangle_k$, as functions of the coupling strength d.

symbol probability

$$\Omega_\beta = \frac{1}{N}\sum_{\tau=1}^{N_\tau}\left(\frac{1}{N_\tau}\sum_{i=1}^{N}\delta_{\sigma_\tau^{(i)},\beta}\right) \tag{8}$$

quantifies the relative frequency of each symbol $\beta \in \{1,\ldots,N_\beta\}$ across all nodes and time windows. For $d = 0$, only the highest symbolic state ($\beta = N_\beta$) is observed. As d increases, additional symbols—representing more regular and less chaotic regimes—are progressively visited. Each symbol reaches its maximum occurrence at a specific coupling value [Fig. 5(a)], revealing a *hierarchical ordering* in which less chaotic regimes peak later along the route to synchronization. As d approaches the critical value where Φ_σ collapses ($d \sim 0.22$), the distribution reconverges toward $\Omega_{N_\beta} \approx 1$, indicating that CI has effectively ceased.

Figure 5(b) provides clear evidence of topologically induced dynamical differentiation [58,59]. We define the *degree-class symbolic average* as

$$\langle\sigma\rangle_k = \frac{1}{|C_k|N_\tau}\sum_{i\in C_k}\sum_{\tau=1}^{N_\tau}\sigma_\tau^{(i)}, \tag{9}$$

where C_k is the set of nodes with degree k. The results show that the regimes accessible to each node depend strongly on its topological role: Highly connected nodes (hubs) explore a broader set of regimes and settle earlier into less chaotic ones, whereas low-degree nodes remain mostly confined to regimes close to the original chaotic one. This degree-dependent differentiation produces a clear hierarchy in symbol exploration, linking topological heterogeneity to dynamical specialization during the collapse of itinerancy.

This degree-dependent differentiation may have broader implications for understanding how itinerant dynamics organize and interact in heterogeneous systems, including large-scale brain dynamics or reservoir computing architectures, where structured heterogeneity enhances computational flexibility and memory capacity.

Functional symbolic synchronization

The symbolic representation introduced above is not limited to quantifying CI, but it also provides a tool for uncovering coordination patterns that remain hidden to approaches based solely on instantaneous phase or amplitude correlations. This perspective enables the definition of *symbolic synchronization*, a state in which nodes coordinate their dynamics even in the absence of other forms of synchrony. We therefore investigate the extent to which nodes exhibit coordinated symbolic transitions and how these patterns relate to their structural roles.

Figure 6(a) shows the *functional symbolic synchronization matrix*, S_σ, for the same ensemble of oscillators analyzed in Sec. III, computed at a representative coupling within the chaotic itinerancy regime ($d = 0.024$). Each matrix element is the normalized Hamming correlation of the respective symbolic sequences:

$$S_\sigma^{(i,j)} = \frac{1}{N_\tau}\sum_{\tau=1}^{N_\tau}\delta_{\sigma_\tau^{(i)},\sigma_\tau^{(j)}}. \tag{10}$$

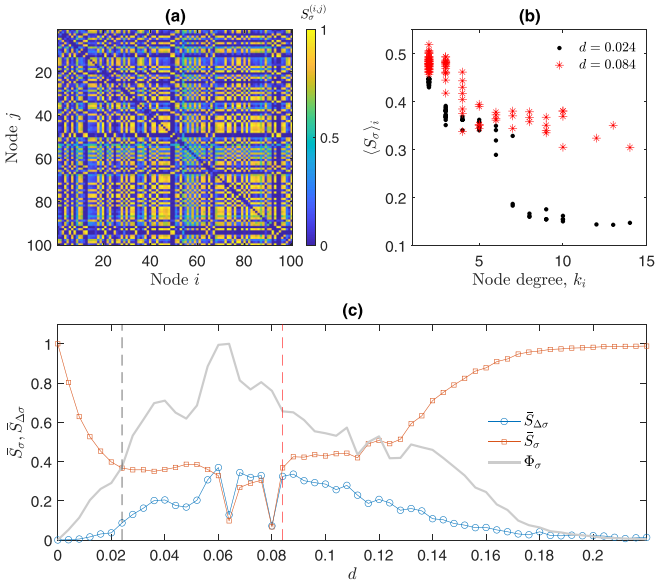


FIG. 6. Functional symbolic synchronization in a network of chaotic Rössler oscillators. (a) Functional symbolic synchronization matrix $S_\sigma^{(i,j)}$ for the same network realization used in Fig. 3 for $d = 0.024$. (b) Average functional symbolic synchronisation of each node with its neighbors, $\langle S_\sigma\rangle_i$, as a function of the node degree k_i for two coupling values indicated by vertical lines in panel (c). (c) Global averages of symbolic state synchronization, $\bar{S}_\sigma$, and the symbolic transition synchronization, $\bar{S}_{\Delta\sigma}$, vs coupling d. The chaotic itinerancy index Φ_σ is shown in gray for reference.

High values of $S_\sigma^{(i,j)}$ indicate frequent symbolic coordination, even in the absence of direct signal synchronization.

The resulting patterns reveal that nodal symbolic synchronization can emerge well before global coherence, uncovering latent forms of coordination driven by the network. These patterns can provide insights into the underlying topology, even for very weak couplings. Figure 6(b) displays the average symbolic synchronization of each node with its neighbors, $\langle S_\sigma\rangle_i = N^{-1}\sum_j S_\sigma^{(i,j)}$, as a function of its degree k_i for two representative coupling strengths [marked by vertical lines in Fig. 6(c)]. The observed monotonic decrease of $\langle S_\sigma\rangle_i$ with k_i indicates that hubs synchronize their regimes less than low-degree nodes, reflecting the degree-dependent range of symbol exploration [Fig. 5(b)].

However, as shown above, we can describe another possible level of coordination in the weakly coupled regime: the *itinerancy synchronization*, where nodes change their symbols simultaneously. To disentangle this process from the symbolic synchronization, we compute

$$S_{\Delta\sigma}^{(i,j)} = \frac{1}{N_\tau - 1}\sum_{\tau=1}^{N_\tau-1}\chi_\tau^{(i)}\,\chi_\tau^{(j)}, \tag{11}$$

where $\chi_\tau^{(i)} = 1 - \delta_{\sigma_{\tau+1}^{(i)},\,\sigma_\tau^{(i)}}$ is a binary indicator that takes the value 1 whenever node i changes symbolic state between consecutive windows, and 0 otherwise.

This quantity captures whether nodes perform synchronous symbol switches, regardless of the states they occupy before or after the transition. To compare the two types of

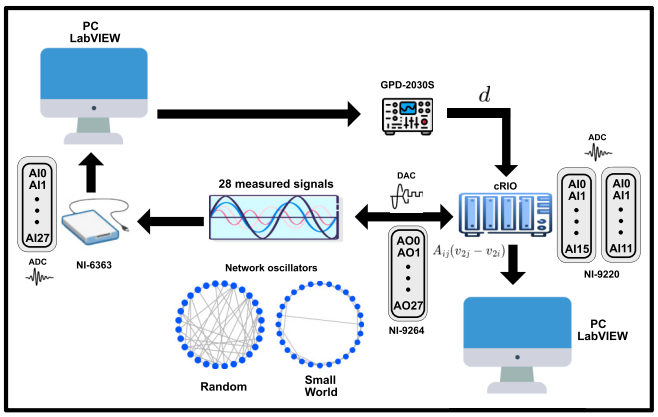


FIG. 7. Schematic of the hybrid experimental acquisition and feedback system. Electronic Rössler-like oscillators are interfaced with both a CompactRIO (cRIO-9074) embedded platform and a DAQ board (NI-6363) via their voltage outputs. The CompactRIO performs real-time processing to compute diffusive coupling terms from instantaneous node states and generates feedback signals according to a prescribed adjacency matrix. The global coupling strength d is adjusted through an analog control voltage supplied by a programmable power source (GPD-2030S). Signals are recorded by the DAQ (sampling rate 50 kHz) for offline analysis, and the entire setup is automated using LabVIEW. The hybrid (cRIO+DAQ) architecture enables precise, repeatable sweeps of d and flexible real-time implementation of different topologies.

synchronization, Fig. 6(c) shows the evolution, as a function of the coupling, of the mean values of the matrices given by Eqs. (10) and (11), $\bar{S}_\sigma$ and $\bar{S}_{\Delta\sigma}$, respectively. In the CI regime (with Φ_σ also plotted as a reference), $\bar{S}_{\Delta\sigma}$ rises sharply, showing that transitions become temporally aligned across the network, even though $\bar{S}_\sigma$ remains lower because nodes often occupy different symbols. At the end of CI, $\bar{S}_\sigma$ increases again as all nodes converge to the same symbol, while $\bar{S}_{\Delta\sigma}$ returns to zero once transitions cease. This provides a functional viewpoint on how coherence develops in complex networks as a multistage process: First, nodes synchronize the *timing* of regime switches (transition synchrony), and later they stabilize into the same symbols (state synchrony).

V. EXPERIMENTAL EVIDENCE

To experimentally test our predictions, we built a hybrid electronic network composed of $N = 28$ analog oscillators emulating Rössler-like chaotic dynamics. The oscillators were interconnected through resistive links enabling adjustable diffusive coupling, with the effective coupling strength d controlled externally by a programmable voltage source. Signal acquisition and feedback operations were handled by a real-time control platform (National Instruments CompactRIO) equipped with high-resolution data acquisition, ensuring precise monitoring and tuning of the local and collective dynamics. The experimental data are available in Refs. [60,61].

This hybrid architecture provides precise and repeatable control of the coupling strength, as well as arbitrary reconfiguration of the network connectivity. In this study, we implemented networks of $N = 28$ nodes generated according

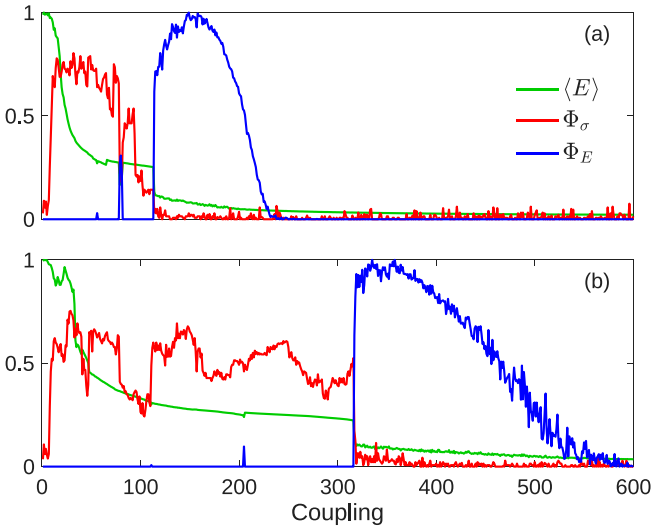


FIG. 8. Normalized mean synchronization error $\langle E \rangle$ (green), chaotic itinerancy index Φ_β (red), and synchronization index Φ_E (blue) in the experimental $N = 28$, $\langle k \rangle = 4$ networks with two different topologies: (a) Erdös-Renyi and (b) Watts-Strogatz with rewiring probability $p = 0.1$. Analysis parameters: $N_\beta = 6$, $D = 100$, and $\theta_E = 0.02$.

to the Watts-Strogatz model [62], with an average degree $\langle k \rangle = 4$ and two levels of randomness: $p = 1$, corresponding to an Erdős-Rényi-like topology, and $p = 0.1$, which preserves some clustering while remaining largely random. Figure 7 summarizes the experimental platform and real-time control scheme, while additional details are provided in the Supplemental Material [44].

Figure 8 presents the experimental measurements of the chaotic itinerancy index Φ_σ, the intermittent synchronization index Φ_E, and the average synchronization error $\langle E \rangle$ as functions of the applied coupling for the two implemented topologies. Although the experimental error $\langle E \rangle$ remains finite due to noise and component mismatches, both indices display a clear and robust crossover: at low coupling $\Phi_\sigma > \Phi_E$ (itinerancy-dominated dynamics), whereas at stronger coupling $\Phi_E > \Phi_\sigma$ (intermittency-dominated dynamics). These observations confirm that the sequence of CI and IS is not limited to numerical models but constitutes a robust and reproducible feature of real-world weakly coupled chaotic networks.

VI. CONCLUSIONS

In this work, we demonstrated that the route to synchronization in complex networks of chaotic oscillators unfolds through two successive and distinct dynamical phenomena: CI and IS. Although both phenomena have been previously reported, they are often regarded as manifestations of the same underlying process. Our results, however, reveal that CI and IS represent *mutually exclusive stages*, each governed by distinct dynamical mechanisms and critical properties, and occurring within separate intervals of the coupling strength.

By introducing a symbolic dynamics approach, we provided a nodal-level characterization of CI as a collective

yet unsynchronized exploration of metastable regimes that constitute each node's subattractor. CI, which had not been systematically investigated in heterogeneous networks, is shown to depend strongly on structural diversity: Networks with broader degree distributions exhibit richer itinerant dynamics, and high-degree nodes access a larger set of regimes than low-degree nodes. A symbolic functional synchronization analysis further shows that, during CI, nodes tend to synchronize their *transitions* before their *regimes*, highlighting a form of temporal coordination that precedes global coherence. The subsequent alignment of symbolic states marks the onset of IS, preceding full synchronization.

As coupling increases, CI vanishes and gives way to IS, where the network alternates irregularly between synchronous and asynchronous phases, displaying on-off intermittency. Both regimes exhibit power-law residence times, indicating that critical organization shapes the entire synchronization route. The transition between these phenomena occurs within a consistent coupling interval across network topologies and oscillator types, suggesting a robust and possibly general scenario. Analysis of the Lyapunov spectrum across this transition reveals a direct correspondence between the two phenomena and the hierarchical reduction of dimensionality that accompanies the emergence of collective order. Experimental implementations in electronic oscillator networks reproduce these features, confirming that the two-step sequence CI-IS is not only a theoretical construct but a generic route observed in real systems.

Beyond its theoretical relevance, the sequential organization of critical regimes identified here may be the key to understanding flexible coordination in biological and artificial systems. In the brain, CI and IS have been proposed as mechanisms for cognitive flexibility and information routing [4,15]. Similarly, in reservoir computing and neuromorphic architectures, operating near the transition between CI and IS may enhance computational capacity and adaptability [33–35]. The potential functional role of CI in realistic settings is determined by its response to noise, a particularly delicate aspect in metastable regimes, as such perturbations can induce both destructive [63] or constructive effects, including resonance phenomena [64]. Our experimental results in Sec. V indicate that CI exhibits tolerance to a certain level of noise. The robustness of CI against noise has likewise been observed in other systems [8], and in many cases, it is even considered an inductive or facilitating mechanism for CI [45,65]. Future research will address how a noisy environment modifies and constrains the scenario developed in the present work.

Overall, our results provide a unified framework linking transient, metastable, and critical dynamics in complex networks, highlighting the fundamental role of structural heterogeneity in shaping the route to synchronization.

ACKNOWLEDGMENTS

I.L., I.S., and C.L. acknowledge support from the Spanish Ministerio de Ciencia e Innovación under Project No. PID2023-147827NB-I00. R.S.E acknowledges support from the Consejo Nacional de Ciencia y Tecnología, México, SEP-CONACYT/CB-2016-01, Grant No. 285909. V.P.V.A. acknowledges financial support from Secretaría de Investigación y Posgrado (SIP), Instituto Politécnico Nacional (IPN) under Research Initiation Project No. 20253622.

DATA AVAILABILITY

The data that support the findings of this article are openly available [60,61].

[1] J. M. Beggs and D. Plenz, Neuronal avalanches in neocortical circuits, J. Neurosci. **23**, 11167 (2003).

[2] W. L. Shew and D. Plenz, The functional benefits of criticality in the cortex, Neuroscientist **19**, 88 (2013).

[3] M. A. Muñoz, *Colloquium*: Criticality and dynamical scaling in living systems, Rev. Mod. Phys. **90**, 031001 (2018).

[4] R. Calvo, C. Martorell, G. B. Morales, S. Di Santo, and M. A. Muñoz, Frequency-dependent covariance reveals critical spatiotemporal patterns of synchronized activity in the human brain, Phys. Rev. Lett. **133**, 208401 (2024).

[5] S. A. Kauffman, *The Origins of Order: Self-Organization and Selection in Evolution* (Oxford University Press, Oxford, 1993).

[6] R. Solé and J. Bascompte, *Self-Organization in Complex Ecosystems* (Princeton University Press, Princeton, 2012).

[7] N. Bertschinger and T. Natschläger, Real-time computation at the edge of chaos in recurrent neural networks, Neural Comput. **16**, 1413 (2004).

[8] F. Hancock, F. E. Rosas, A. I. Luppi, M. Zhang, P. A. M. Mediano, J. Cabral, G. Deco, M. L. Kringelbach, M. Breakspear, J. A. S. Kelso, and F. E. Turkheimer, Metastability demystified—The foundational past, the pragmatic present and the promising future, Nat. Rev. Neurosci. **26**, 82 (2025).

[9] I. Tsuda, Dynamic link of memory—Chaotic memory map in nonequilibrium neural networks, Neural Networks **5**, 313 (1992).

[10] L. M. Kay, A challenge to chaotic itinerancy from brain dynamics, Chaos **13**, 1057 (2003).

[11] V. P. Vera-Ávila, J. R. Sevilla-Escoboza, and I. Leyva, Complex networks exhibit intermittent synchronization, Chaos **30**, 103119 (2020).

[12] A. Choudhary, C. Mitra, V. Kohar, S. Sinha, and J. Kurths, Small-world networks exhibit pronounced intermittent synchronization, Chaos **27**, 111101 (2017).

[13] N. Platt, E. A. Spiegel, and C. Tresser, On-off intermittency: A mechanism for bursting, Phys. Rev. Lett. **70**, 279 (1993).

[14] J. F. Heagy, N. Platt, and S. M. Hammel, Characterization of on-off intermittency, Phys. Rev. E **49**, 1140 (1994).

[15] M. Breakspear, Dynamic models of large-scale brain activity, Nat. Neurosci. **20**, 340 (2017).

[16] F. S. Borges, E. C. Gabrick, P. R. Protachevicz, G. S. V. Higa, E. L. Lameu, P. X. R. Rodriguez, M. S. A. Ferraz, J. D. Szezech, A. M. Batista, and A. H. Kihara, Intermittency properties in a temporal lobe epilepsy model, Epilepsy Behav. **139**, 109072 (2023).

[17] K. Kaneko and I. Tsuda, Chaotic itinerancy, Chaos **13**, 926 (2003).

[18] I. Tsuda, Chaotic itinerancy and its roles in cognitive neurodynamics, Curr. Opin. Neurobiol. **31**, 67 (2015).

[19] D. Koch, A. Nandan, G. Ramesan, and A. Koseska, Biological computations: Limitations of attractor-based formalisms and the need for transients, Biochem. Biophys. Res. Commun. **720**, 150069 (2024).

[20] K. Kaneko, Clustering, coding, switching, hierarchical ordering, and control in a network of chaotic elements, Physica D **41**, 137 (1990).

[21] W. J. Freeman, Evidence from human scalp electroencephalograms of global chaotic itinerancy, Chaos **13**, 1067 (2003).

[22] K. Otsuka, Chaotic itinerancy in a coupled-element multistable optical chain, Phys. Rev. A **43**, 618 (1991).

[23] R. Iwami, T. Mihana, K. Kanno, S. Sunada, M. Naruse, and A. Uchida, Controlling chaotic itinerancy in laser dynamics for reinforcement learning, Sci. Adv. **8**, eabn8325 (2022).

[24] J.-J. Aucouturier, Y. Ogai, and T. Ikegami, Making a robot dance to music using chaotic itinerancy in a network of Fitzhugh-Nagumo neurons, in *International Conference on Neural Information Processing* (Springer, Berlin Heidelberg, 2008), pp. 647–656.

[25] S. Steingrube, M. Timme, F. Wörgötter, and P. Manoonpong, Self-organized adaptation of a simple neural circuit enables complex robot behaviour, Nat. Phys. **6**, 224 (2010).

[26] J. Park, H. Mori, Y. Okuyama, and M. Asada, Chaotic itinerancy within the coupled dynamics between a physical body and neural oscillator networks, PLoS One **12**, e0182518 (2017).

[27] S. Recanatesi, U. Pereira-Obilinovic, M. Murakami, Z. Mainen, and L. Mazzucato, Metastable attractors explain the variable timing of stable behavioral action sequences, Neuron **110**, 139 (2022).

[28] T. Sasaki, N. Matsuki, and Y. Ikegaya, Metastability of active CA3 networks, J. Neurosci. **27**, 517 (2007).

[29] M. Morrison and L.-S. Young, Chaotic heteroclinic networks as models of switching behavior in biological systems, Chaos **32**, 123102 (2022).

[30] J. A. Roberts, L. L. Gollo, R. G. Abeysuriya, G. Roberts, P. B. Mitchell, M. W. Woolrich, and M. Breakspear, Metastable brain waves, Nat. Commun. **10**, 1056 (2019).

[31] P. Ashwin, M. Fadera, and C. Postlethwaite, Network attractors and nonlinear dynamics of neural computation, Curr. Opin. Neurobiol. **84**, 102818 (2024).

[32] K. L. Rossi, R. C. Budzinski, E. S. Medeiros, B. R. Boaretto, L. Muller, and U. Feudel, Dynamical properties and mechanisms of metastability: A perspective in neuroscience, Phys. Rev. E **111**, 021001 (2025).

[33] K. Inoue, K. Nakajima, and Y. Kuniyoshi, Designing spontaneous behavioral switching via chaotic itinerancy, Sci. Adv. **6**, eabb3989 (2020).

[34] L.-W. Kong, G. A. Brewer, and Y.-C. Lai, Reservoir-computing based associative memory and itinerancy for complex dynamical attractors, Nat. Commun. **15**, 4840 (2024).

[35] J. O'Hagan, A. Keane, and A. Flynn, Confabulation dynamics in a reservoir computer: Filling in the gaps with untrained attractors, Chaos **35**, 093130 (2025).

[36] T. Kabayama, M. Komuro, Y. Kuniyoshi, K. Aihara, and K. Nakajima, Crisis-induced intermittency in reservoir computing, Phys. Rev. Res. **7**, L032058 (2025).

[37] A. Mattera, V. Alfieri, G. Granato, and G. Baldassarre, Chaotic recurrent neural networks for brain modelling: A review, Neural Networks **184**, 107079 (2025).

[38] S. Uchiyama and H. Fujisaka, Wandering behavior of the chaotic itinerancy in an oscillator neural network model, Prog. Theor. Phys. Suppl. **161**, 381 (2006).

[39] J. J. Torres, J. Marro, J. M. Cortes, and B. Wemmenhove, Instabilities in attractor networks with fast synaptic fluctuations and partial updating of the neurons activity, Neural Networks **21**, 1272 (2008).

[40] A. A. Khatun, Y. A. Muthanna, N. Punetha, and H. H. Jafri, Collective dynamics of coupled Lorenz oscillators near the Hopf boundary: Intermittency and chimera states, Phys. Rev. E **109**, 034208 (2024).

[41] T. Sameshima, K. Fukushima, H. Shibata, and T. Yamada, Lyapunov spectrum analysis for a chaotic transition phenomenon, Europhys. Lett. **62**, 21 (2003).

[42] A.-L. Barabási and R. Albert, Emergence of scaling in random networks, Science **286**, 509 (1999).

[43] P. Erdős and A. Rényi, On random graphs, Publ. Math. Debrecen **6**, 290 (1959).

[44] See Supplemental Material at http://link.aps.org/supplemental/10.1103/s3gp-gtln for examples of CI in other models and additional data about the experimental setup.

[45] M. Timme, F. Wolf, and T. Geisel, Prevalence of unstable attractors in networks of pulse-coupled oscillators, Phys. Rev. Lett. **89**, 154105 (2002).

[46] D. J. Gauthier and J. C. Bienfang, Intermittent loss of synchronization in coupled chaotic oscillators: Toward a new criterion for high-quality synchronization, Phys. Rev. Lett. **77**, 1751 (1996).

[47] S. Boccaletti and D. L. Valladares, Characterization of intermittent lag synchronization, Phys. Rev. E **62**, 7497 (2000).

[48] G. Benettin, L. Galgani, A. Giorgilli, and J.-M. Strelcyn, Lyapunov characteristic exponents for smooth dynamical systems and for Hamiltonian systems; a method for computing all of them. Part 2: Numerical application, Meccanica **15**, 21 (1980).

[49] R. Gutiérrez, R. Sevilla-Escoboza, P. Piedrahita, C. Finke, U. Feudel, J. M. Buldú, G. Huerta-Cuellar, R. Jaimes-Reátegui, Y. Moreno, and S. Boccaletti, Generalized synchronization in relay systems with instantaneous coupling, Phys. Rev. E **88**, 052908 (2013).

[50] J. L. Kaplan and J. A. Yorke, Chaotic behavior of multidimensional difference equations, in *Functional Differential Equations and Approximation of Fixed Points*, edited by H.-O. Peitgen and H.-O. Walther (Springer, Berlin, 1979), pp. 204–227.

[51] K. Kaneko, Information cascade with marginal stability in a network of chaotic elements, Physica D **77**, 456 (1994).

[52] I. Tsuda, H. Fujii, S. Tadokoro, T. Yasuoka, and Y. Yamaguti, Chaotic itinerancy as a mechanism of irregular changes between synchronization and desynchronization in a neural network, J. Integr. Neurosci. **03**, 159 (2004).

[53] G. Tirabassi, R. Aristides, C. Masoller, and D. J. Gauthier, Bubbling in oscillator networks, arXiv:2504.07374.

[54] J. Namikawa, Chaotic itinerancy and power-law residence time distribution in stochastic dynamical systems, Phys. Rev. E **72**, 026204 (2005).

[55] H. Fujisaka and T. Yamada, Stability theory of synchronized motion in coupled-oscillator systems, Prog. Theor. Phys. **69**, 32 (1983).

[56] P. W. Hammer, N. Platt, S. M. Hammel, J. F. Heagy, and B. D. Lee, Experimental observation of on-off intermittency, Phys. Rev. Lett. **73**, 1095 (1994).

[57] S. C. Venkataramani, T. M. Antonsen, E. Ott, and J. C. Sommerer, Characterization of on-off intermittent time series, Phys. Lett. A **207**, 173 (1995).

[58] A. Tlaie, I. Leyva, R. Sevilla-Escoboza, V. P. Vera-Avila, and I. Sendiña-Nadal, Dynamical complexity as a proxy for the network degree distribution, Phys. Rev. E **99**, 012310 (2019).

[59] C. Letellier, I. Sendiña-Nadal, L. Minati, and I. Leyva, Node differentiation dynamics along the route to synchronization in complex networks, Phys. Rev. E **104**, 014303 (2021).

[60] J. R. Sevilla-Escoboza, V. P. Vera-Avila, I. Leyva, and R. R. Rivera-Durón, Experimental datasets on intermittency in networks of electronic oscillators. Hybrid configuration—Random (Erdös-Rényi) topology, Zenodo (2025), https://doi.org/10.5281/zenodo.17451096.

[61] J. R. Sevilla-Escoboza, V. P. Vera Avila, R. R. Rivera-Durón, and I. Leyva, Experimental datasets on intermittency in networks of electronic oscillators. Hybrid configuration—Small-world (Watts-Strogatz), Zenodo (2025), https://doi.org/10.5281/zenodo.17451530.

[62] D. J. Watts and S. H. Strogatz, Collective dynamics of 'small-world' networks, Nature (London) **393**, 440 (1998).

[63] C. Nathe, C. Pappu, N. A. Mecholsky, J. Hart, T. Carroll, and F. Sorrentino, Reservoir computing with noise, Chaos **33**, 041101 (2023).

[64] K. Kitajo, S. M. Doesburg, K. Yamanaka, D. Nozaki, L. M. Ward, and Y. Yamamoto, Noise-induced large-scale phase synchronization of human-brain activity associated with behavioural stochastic resonance, Europhys. Lett. **80**, 40009 (2007).

[65] J. Matulis and H. Bindra, Effect of stochasticity on initial transients and chaotic itinerancy for a natural circulation loop, Phys. Rev. E **112**, 044223 (2025).